

1
2
3
4
5
6
7
8
9
10
11
12
13
14
15
16
17
18
19
20
21
22
23
24
25
26

**Regional Measurements and Spatial/Temporal Analysis of CDOM in 10,000+ Optically
Variable Minnesota Lakes using Landsat 8 Imagery**

Leif G. Olmanson^{1*}, Benjamin P. Page², Jacques C. Finlay³, Patrick L. Brezonik⁴, Marvin E.
Bauer¹, Claire G. Griffin^{3,5}, Raymond M. Hozalski⁴

¹*Department of Forest Resources, University of Minnesota, St. Paul, Minnesota 55108 USA*

²*Water Resources Center, University of Minnesota, St. Paul, Minnesota 55108 USA*

³*Department of Ecology, Evolution and Behavior, University of Minnesota, St. Paul, Minnesota
55108 USA*

⁴*Department of Civil, Environmental, and Geo- Engineering, University of Minnesota,
Minneapolis, Minnesota 55455 USA*

⁵*Department of Environmental Sciences, University of Virginia, Charlottesville, Virginia 22905
USA*

*Corresponding author. E-mail: olman002@umn.edu

27 **Abstract**

28 Information on colored dissolved organic matter (CDOM) is essential for understanding and
29 managing lakes but is often not available, especially in lake-rich regions where concentrations
30 are often highly variable in time and space. We developed remote sensing methods that can use
31 both Landsat and Sentinel satellite imagery to provide census-level CDOM measurements across
32 the state of Minnesota, USA, a lake-rich landscape with highly varied lake, watershed, and
33 climatic conditions. We evaluated the error of satellite derived CDOM resulting from two
34 atmospheric correction methods with in situ data, and found that both provided substantial
35 improvements over previous methods. We applied CDOM models to 2015 and 2016 Landsat 8
36 OLI imagery to create 2015 and 2016 Minnesota statewide CDOM maps (reported as absorption
37 coefficients at 440 nm, a_{440}) and used those maps to conduct a geospatial analysis at the
38 ecoregion level. Large differences in a_{440} among ecoregions were related to predominant land
39 cover/use; lakes in ecoregions with large areas of wetland and forest had significantly higher
40 CDOM levels than lakes in agricultural ecoregions. We compared regional lake CDOM levels
41 between two years with strongly contrasting precipitation (close-to-normal precipitation year in
42 2015 and much wetter conditions with large storm events in 2016). CDOM levels of lakes in
43 agricultural ecoregions tended to decrease between 2015 and 2016, probably because of dilution
44 by rainfall, and 7% of lakes in these areas decreased in a_{440} by $\geq 3 \text{ m}^{-1}$. In two ecoregions with
45 high forest and wetlands cover, a_{440} increased by more than 3 m^{-1} in 28 and 31% of the lakes,
46 probably due to enhanced transport of CDOM from forested wetlands. With appropriate model
47 tuning and validation, the approach we describe could be extended to other regions, providing a
48 method for frequent and comprehensive measurements of CDOM, a dynamic and important
49 variable in surface waters.

50

51 **Keywords:** Satellite remote sensing, water color, atmospheric correction, water quality
52 monitoring, lake management, inland waters

53

54 **1. Introduction**

55 Research in recent decades has revealed a central role for colored (or chromophoric)
56 dissolved organic matter (CDOM) in regulating major physical, chemical and biological
57 processes in lakes and rivers (e.g., reviewed in Solomon et al. 2015, Williamson et al. 1999,
58 Creed et al. 2018, and elsewhere). We now know that CDOM functions as one of a small number
59 of "master variables," similar to phosphorus, pH and redox potential, that control important
60 aspects of the composition and functioning of aquatic ecosystems and regulate their responses to
61 environmental change (Williamson et al. 1999, Creed et al. 2018). Recent studies show that
62 CDOM levels strongly influence: (a) light and thermal regimes in lakes (e.g., Houser 2006, Ask
63 et al. 2009, Thrane et al. 2014, Pilla et al. 2018, Snucins and Gunn 2000), (b) biogeochemical
64 cycles (e.g., Knoll et al. 2018, Corman et al. 2018), (c) food web processes and interactions (e.g.,
65 Karlsson et al. 2009, Solomon et al. 2015), (d) contaminant bioavailability (e.g., Tsui and Finlay
66 2011), and (e) water clarity (e.g., Brezonik et al. 2019a). Knowledge of the sources, levels, and
67 cycling of CDOM in freshwaters thus is important for aquatic resource management and for
68 predicting the outcomes of environmental change.

69 Moderate to high levels of CDOM in freshwaters are determined largely by rates of
70 transport from soils and wetlands in surrounding watersheds and thus are affected by a
71 combination of factors related to vegetation and hydrology. The dependency of aquatic CDOM
72 on dynamic external sources, combined with internal production and loss processes in aquatic

73 systems, can lead to high variability of CDOM levels across landscapes and within lakes at time
74 scales of seasons to years (Brezonik et al. 2015, Williamson, et al. 2015). Human-driven changes
75 in temperature, atmospheric chemistry, land use and watershed hydrology also can have strong
76 effects on CDOM (Creed et al. 2018, Finstad et al. 2016, Kritzberg 2017, Stanley et al. 2012, de
77 Wit 2018).

78 Although CDOM is easily measured in the laboratory, the availability of in situ CDOM
79 data is surprisingly limited relative to its importance, even in states like Minnesota, where
80 monitoring of its > 10,000 surface waters is a major focus of many state, tribal and local
81 agencies. Several recent, large-scale assessments of regional U.S. lake monitoring efforts
82 (Stanley et al. 2012; Ross et al. 2019) showed that far fewer data were available for CDOM and
83 related variables such as DOC compared to nutrients, chlorophyll, and water clarity, despite the
84 strong effects of CDOM on those and other physicochemical variables. The spatial and temporal
85 variation in CDOM in surface waters suggests the need for more CDOM data to improve
86 understanding of drivers and better predict lake responses to stresses ranging from local land-
87 cover changes to global climate change. Some countries with large numbers of CDOM-rich lakes
88 have incorporated routine monitoring of CDOM or a related parameter such as DOC (e.g., Sobek
89 et al. 2007). The relative lack of CDOM data for U.S. lakes (Stanley et al. 2019) may stem from
90 the fact that many monitoring programs initially started in relatively low-CDOM regions but also
91 from the fact that the importance of CDOM as a driver of ecological conditions has been
92 appreciated only recently.

93 Whatever the cause, the availability of CDOM data remains deficient compared to its
94 importance. Remote sensing using satellite-based sensors could play an important role in
95 providing CDOM data at high temporal and spatial resolution. Recent studies show that the

96 Landsat sensors (Kutser et al. 2005, Brezonik et al. 2005, Kutser et al. 2009, Olmanson et al.
97 2016a), and Sentinel-2/MSI sensors (Toming et al. 2016, Chen et al. 2017) can provide such data
98 at scales relevant for inland lakes as small as 4 hectares (ha).

99 Recent improvements in Earth-observing satellite sensors have expanded the capabilities
100 to measure optically-related water quality characteristics, including CDOM, in lakes (Olmanson
101 et al. 2016a; Tyler et al. 2016, Pahlevan et al. 2019, Page et al. 2019). Specifically, the Landsat 8
102 Operational Land Imager (L8/OLI) and the European Space Agency (ESA) Sentinel-2
103 MultiSpectral Imager (S2/MSI) have improved spatial, spectral, radiometric and temporal
104 resolution compared with earlier sensors. With the L8/OLI and S2/MSI constellation collecting
105 imagery every 3 to 5 days, frequent satellite-based measurements of a variety of key water
106 quality variables on lakes are now possible.

107 The use of satellite imagery to measure CDOM at large regional scales and over multiple
108 time periods requires analysis of multiple images. Unless ground-based data are available to
109 calibrate each image (a requirement difficult to achieve), accurate methods are needed for
110 atmospheric correction of images to produce surface reflectance data directly representative of
111 optical signals from waterbodies. Although various approaches have been reported to accomplish
112 this (e.g., Pahlevan et al. 2017a,b and Vanhellemont and Ruddick 2015, 2016), we have found
113 that many of them yield unreliable results for inland lakes (Olmanson et al. 2011, Page et al.
114 2019). The recent availability of surface reflectance products from the EROS Center appears to
115 have overcome this obstacle for Landsat 8 imagery (Kuhn et al. 2019), and Page et al. (2019)
116 described a workflow process to atmospherically correct and harmonize S2/MSI and L8/OLI
117 satellite imagery in Google's Earth Engine (GEE) (Gorelick et al. 2017).

118 This paper describes application of these advances to measure CDOM on all waterbodies

119 larger than 4 ha across a large geographic region (the state of Minnesota) that encompasses more
120 than 226,000 km² and contains officially 11,842 lakes 4 ha or larger in area
121 (<https://www.dnr.state.mn.us/faq/mnfacts/water.html>). The paper describes a robust semi-
122 empirical approach for routine monitoring of CDOM using L8/OLI imagery. We demonstrate the
123 consistency and reliability of two atmospheric correction methods to generate remote sensing
124 reflectance (R_{rs}) products and use these products to assemble a CDOM database on more than
125 10,500 lakes for both 2015 and 2016. We assess the accuracy of retrieved CDOM data for both
126 low- and high-CDOM waters and summarize distributions of CDOM in Minnesota lakes at the
127 ecoregion level.

128

129 **2. Methods**

130 *2.1 Study area*

131 Minnesota, a large, lake-rich state in the Upper Midwest of the U.S., comprises parts of
132 seven ecoregions (Omernik and Griffith 2014) that differ in land-cover, geology, soils,
133 vegetation and hydrologic conditions (Figure 1). Known popularly as “the land of 10,000 lakes,”
134 Minnesota actually has approximately 12,000 waterbodies with surface areas ≥ 4 ha (Olmanson
135 et al. 2014) and many more that are smaller than that. The lakes are distributed broadly (but not
136 uniformly) across the ecoregions. Two ecoregions, the Northern Lakes and Forests (NLF) and
137 North Central Hardwood Forest (NCHF), together comprise 49% of the state’s area and contain
138 84% of the state’s lakes (47% and 37%, respectively). According to Olmanson et al. (2014),
139 about one-fourth of the heavily forested NLF (mixed conifers and hardwoods) is wetlands and
140 lakes; only 4% is urban and 7% agricultural land. The high proportion of forest (66%) and
141 wetlands (14%) leads to high CDOM levels in many NLF surface waters (Griffin et al. 2018;

142 Brezonik et al. 2019a,b). In contrast, half of the NCHF is agricultural land, and about 10% is
143 urban or suburban; forests account for only about 17% of the ecoregion, and wetlands constitute
144 11% of the landscape.

145 The Western Corn Belt Plain (WCBP) occupies most of southern Minnesota and is
146 dominated (~ 77%) by row-crop agriculture (mainly corn and soybean); its land-cover is only ~
147 7% forested. The Northern Glaciated Plains (NGP) ecoregion occupies a small region of
148 southwest Minnesota and is similar to the WCBP in agricultural land cover (74%) but has a
149 higher percentage of grassland (9%). Together, the WCBP and NGP contain 12% of the state's
150 lakes. The Lake Agassiz Plain (LAP) ecoregion (Omernik and Griffith 2014), formerly called the
151 Red River Valley ecoregion (Omernik 1987), has the highest percentage (84%) of agricultural
152 land among the state's ecoregions, and the flat land is a remnant of glacial Lake Agassiz. This
153 ecoregion has only 215 lakes (2% of the state's total). The Northern Minnesota Wetlands
154 (NMW) ecoregion is contiguous to the NLF and is similarly heavily forested (52%). The NMW
155 has more wetlands (19%), however, and its flat landscape contains few lakes, although three of
156 the state's largest lakes, Upper and Lower Red Lake and Lake of the Woods, are in the NMW.
157 The non-glaciated Driftless Area in southeastern Minnesota has only a few small manmade
158 ponds and reservoirs and backwater areas of the Mississippi River.

159

160 *2.2 Calibration data*

161 A dataset of ground-based CDOM levels for satellite imagery calibration was developed
162 from our ongoing CDOM studies (e.g., Griffin et al. 2018, Brezonik et al. 2019a,b) and includes
163 data from the Minnesota Pollution Control Agency (MPCA) and several other agencies and
164 collaborators. Sampling in 2015 was focused in the NLF and NCHF in northern Minnesota

165 (Figure 1) and was expanded to include the NMW ecoregion in 2016 and the WCBP, NGP, and
166 LAP ecoregions in 2017. Most lakes were sampled only once, but a selection of lakes were
167 sampled once each year and a few were sampled approximately monthly in 2016 or 2017.
168 Details of sampling were provided previously (Griffin et al. 2018; Brezonik et al. 2019). All
169 observations (site-date combinations) were treated separately; i.e., multiple samples from a
170 lake were not averaged. A total of 1,586 CDOM measurements were collected over 2015-2018,
171 many from routine monitoring efforts by collaborators (Brezonik et al. 2019a). These efforts
172 provided a large dataset of field measurements for calibration and validation.

173 Sampling procedures and field and laboratory analyses followed standard limnological
174 practices. Detailed methods were described by Griffin et al. (2018). In brief, most water samples
175 were collected from ~ 0.25 m below the lake surface; the MPCA samples were a 0-2 m
176 integrated sample of the epilimnion. Water for CDOM analysis was filtered through 0.45 µm
177 Geotech High Capacity filters and stored in the dark at 4 °C in pre-ashed 40 mL amber glass
178 bottles until analysis within 1 month of collection. Samples for DOC were acidified using 2 M
179 HCl and stored in pre-ashed 20 mL glass bottles at 4°C. Other samples were stored in acid-
180 washed and triple-rinsed polycarbonate or high-density polyethylene bottles and filtered for
181 analysis of various dissolved constituents within 24 h of collection.

182 CDOM was determined from absorbance measurements at 440 nm, using a Shimadzu
183 1601UV-PC dual beam spectrophotometer through 1 or 5 cm quartz cuvettes against a nanopure
184 water blank. Absorbance was converted to Napierian absorption coefficients (Kirk 2010) using:

185
$$a_{440} = 2.303A_{440}/l \quad (1)$$

186 where: a_{440} is the absorption coefficient at 440 nm, A_{440} is absorbance at 440 nm, and l is cell
187 path length (m). Absorbance scans were blank-corrected before conversion. CDOM values are
188 reported as a_{440} (m^{-1}).

189

190 *2.3 Image acquisition and processing*

191 A critical component of image processing for aquatic environments is a consistent
192 atmospheric correction (AC) method that can yield reliable estimates of the surface water-
193 leaving reflectance (ρ_w), an optically active input parameter for various satellite-based water
194 quality models (Gordon and Wang 1994). We evaluated atmospherically corrected L8/OLI
195 remote sensing reflectance ($R_{rs} = \rho_w/\pi$) products derived from the **Modified Atmospheric**
196 **Correction for INland waters (MAIN)** (Page et al. 2019) method implemented in Google Earth
197 Engine (GEE) (Gorelick et al., 2017) to map CDOM in Minnesota lakes. Mean R_{rs} values were
198 extracted from a 50-m buffer around each sample location within the open water area of each
199 lake using a collection of clear imagery from L8/OLI to develop a CDOM retrieval algorithm.
200 Paths of clear L8/OLI imagery with coincident field data from 2015 and 2016 were used for
201 model calibration, and coincident L8/OLI and S2/MSI imagery from 2018 were used with
202 corresponding field data for independent validation of the results. Finally, R_{rs} values from the
203 U.S. Geological Survey Surface Reflectance Product (OLI-SR version 1.3.0) also were evaluated
204 for cross-model comparisons.

205

206 *2.4 CDOM modeling approach*

207 Because CDOM concentrations in most lakes are stable on at least a short-term basis
208 (days to weeks) (e.g., Brezonik et al. 2015), we used calibration/validation data that had been

209 collected within 30 days of imagery. This yielded 250 calibration measurements corresponding
210 to five clear paths of L8/OLI imagery in 2015 and 2016 (Table 1). An additional 157
211 measurements from MAIN-processed coincident Landsat 8 and Sentinel-2 imagery for August
212 13, 2018 were used for independent validation and harmonization of the L8/OLI and S2/MSI
213 sensors (Table 1); 62 of these measurements corresponded with clear L8/OLI imagery and 95
214 corresponded with clear S2/MSI imagery. The calibration set included lakes distributed across
215 the state with a wide range of CDOM ($a_{440} = 0.2\text{-}32.5 \text{ m}^{-1}$). The CDOM range in the validation
216 set fit closely with the calibration set at low to moderate CDOM levels (up to $a_{440} \sim 10 \text{ m}^{-1}$) but
217 lacked higher values (Table A1) because wildfire smoke (originating in California USA and
218 Canada) caused haze interference in northern Minnesota, where the high CDOM lakes occur, for
219 the August 13, 2018 validation imagery.

220 To explore the potential of all available OLI bands and band ratios to predict CDOM,
221 modeled as $\ln(a_{440})$, we used the bootstrap forest technique in JMP Pro 14 SAS Institute (2018)
222 and evaluated the most significant combinations. The calibration dataset of measured a_{440} values
223 corresponding with the five clear L8/OLI image paths was used as the dependent variable
224 (Tables 1 and A1), and MAIN-derived (and OLI-SR) mean R_{rs} values for L8/OLI bands B1-B5
225 and all band-ratio permutations were the independent input variables (26 total terms). The two
226 highest-contributing terms that produced the highest coefficient of determination (R^2) and lowest
227 root mean square error (RMSE) with measured data were identified using step-wise regression
228 and were used to develop the models.

229 To evaluate model predictive capability, the data were divided into four randomized
230 groups. For each possible combination, three groups were used as a training set to develop a
231 correlation, and the remaining group was used as a confirmation set. Performance of the models

232 generated from the four randomly selected calibration/confirmation datasets was evaluated from
233 the coefficient of determination (R^2) and root mean square error (RMSE) for model-predicted vs.
234 measured a_{440} , and the average and range of performance of the four datasets were calculated.

235 As an additional check on the consistency of the model over a broader temporal scale and
236 MAIN harmonization of L8/OLI and S2/MSI R_{rs} values, we applied the model derived from
237 L8/OLI imagery to the independent validation datasets described above (Table 1). Accuracy was
238 compared against measured a_{440} for each validation image using mean absolute error (MAE)

$$239 \quad MAE = \frac{\sum_{i=1}^n |a_{440,sensor} - a_{440,in\ situ}|}{n} \quad (2)$$

240 where $a_{440,sensor}$ is either $a_{440,MSI}$ or $a_{440,OLI}$. MAE = 0 indicates a perfect fit.

241

242 *2.5 Statewide CDOM database*

243 To create the 2015 statewide CDOM map, we used five clear paths (i.e., images from the
244 same path and date but from multiple rows (two to five) to cover the state) of L8/OLI imagery
245 (Table 1). For the 2016 map there were five mostly clear paths from 2015, but because a few
246 areas in western Minnesota did not have any clear imagery in 2016, we also used two clear paths
247 of 2017 L8/OLI imagery to fill in missing areas to complete the 2016 map (Table 1). To produce
248 maps, the validated CDOM model was applied to the corresponding selected MAIN-derived R_{rs}
249 bands in the GEE application program interface (API) (Page et al. 2019) for each path of
250 imagery (Table 1) used for the 2015 and 2016 CDOM maps and exported in GeoTIFF format.
251 The paths were mosaicked into statewide maps using ERDAS Imagine to create 2015 and 2016
252 pixel-level CDOM maps for Minnesota. To create a lake-level database, we used a polygon layer
253 previously constructed (Olmanson et al. 2008) to include all Minnesota lakes, reservoirs and

254 open-water wetlands ≥ 4 ha and the signature editor in ERDAS Imagine to extract a_{440} data for
255 all lakes in the images using the lake polygon layer. The GetHist program (Olmanson et al. 2008)
256 was used to calculate the mean a_{440} values from the middle 70 percent and linked to each lake
257 polygon to create lake-level maps for 2015 and 2016.

258 To compile the data for analysis of CDOM at the ecoregion level, we used Esri ArcMap
259 10.5.1 to link each lake polygon to its respective ecoregion, and JMP Pro 14 to calculate CDOM
260 distributions for each Minnesota ecoregion.

261

262 **3. Results and discussion**

263 *3.1 CDOM model results*

264 After exploration of various two-term regression models using L8/OLI, we identified the
265 best model as having the form:

266

$$267 \quad \ln(a_{440}) = a(R_{rs}(B4)/R_{rs}(B3)) + b(R_{rs}(B5)/R_{rs}(B3)) + c \quad (3)$$

268

269 where coefficients, a, b, and c were fit to the calibration data by regression analysis, $\ln(a_{440})$ is
270 the natural logarithm of the L8/OLI-derived a_{440} for a given sample location and B represents the
271 corresponding L8/OLI spectral band. From the combined L8/OLI dataset, the $\ln(a_{440})$ prediction
272 model generated a strong fit with $R^2 = 0.85$ and RMSE = 0.49 for MAIN, and $R^2 = 0.83$ and
273 RMSE = 0.52 for OLI-SR (Table A2, Figure 2). MAIN-based results also fit closer to the 1:1
274 line than OLI-SR results, but both methods provided a better fit in the lower and higher ranges
275 than our previous efforts (Olmanson et al. 2016a, b).

276 To evaluate model performance in different CDOM ranges, we split the data into low,
277 medium and high sets ($a_{440} = 0.2-3.0$, $3-10$ and $10-32.5 \text{ m}^{-1}$, respectively) and calculated MAE
278 (Table 2a). In all ranges, MAIN-corrected imagery had lower MAE values than OLI-SR-
279 corrected imagery, and although the MAE increased with a_{440} , the values were a relatively small
280 fraction of the median a_{440} for the range. We also plotted measured a_{440} from low to high with
281 model predicted a_{440} for MAIN and OLI-SR (Figure 3). MAIN-based results fit closer to the line
282 for field measured a_{440} than OLI-SR results and deviation from the line for field measured a_{440}
283 increased with increasing CDOM.

284 The use of MAIN or OLI-SR image correction together with the best-fit model resulted
285 in substantial improvements in CDOM estimation compared to previous methods, largely due to
286 improved atmospheric correction and a relatively large and varied in situ dataset (Figure 2). In
287 comparison with other models in the literature, the green/red model of Kutser et al. (2005a) and
288 red/green model of Menken et al. (2006) when applied to the combined L8/OLI dataset
289 generated comparatively weak linear regressions with $\ln(a_{440})$: R^2 values of 0.46 and 0.51,
290 respectively, and higher RMSE values of 0.93 and 0.88, respectively (Table A2). The green/blue,
291 red model of Griffin et al. (2011), which uses the blue band, where CDOM absorption is much
292 stronger, generated no convincing relationship (average $R^2 = 0.04$, $\text{RMSE} = 1.24$), which
293 indicates interference from other optically active constituents (Table A2). Compared against
294 previous models, our approach offered substantial improvements in a_{440} measurements especially
295 in the higher and lower ranges.

296

297 *3.2 CDOM model validation*

298 The semi-empirical model developed here was applied to some 2015, 2016 and 2017
299 L8/OLI images that were not used for model development to complete the 2015 and 2016
300 CDOM maps for Minnesota. Because these data do not have in situ validation data it is important
301 to use an independent validation dataset to determine the accuracy that can be expected when the
302 model is used on images not included in the calibration dataset. The validation dataset consists of
303 overlapping L8/OLI and S2/MSI images acquired on August 13, 2018 that were mostly clear but
304 had visible wildfire smoke in northern Minnesota. The L8/OLI validation data for the low and
305 medium CDOM ranges resulted in higher MAE values (1.46 and 2.26 m^{-1} , respectively) than
306 found for the corresponding calibration results (MAE = 0.42 and 1.79 m^{-1} , respectively) using
307 Eq. (2) (Table 2b). The MAE of 1.63 m^{-1} for the whole validation dataset is comparable to that
308 for the calibration dataset with a MAE of 1.61 m^{-1} , likely because of the lack of high CDOM
309 values in the validation data (because the haze problem in northern Minnesota imagery). Despite
310 the lack of high CDOM lakes, the validation data range still represented a large majority (> 92%)
311 of surface waterbodies in Minnesota; CDOM values > 10 m^{-1} occurred in only 8% of the state's
312 surface waters. If we consider only lakes and reservoirs and exclude open-water wetlands (i.e.
313 shallower waterbodies that have abundant aquatic vegetation but include open-water areas where
314 CDOM measurements can be extracted), CDOM > 10 m^{-1} occurred in only 6% of the lakes. The
315 S2/MSI validation dataset yielded larger MAE values of 1.58 and 2.90 m^{-1} (Table 2b) for the low
316 and medium CDOM ranges than corresponding values for the calibration data (0.43 and 2.05 m^{-1} ,
317 Table 2a). The larger errors could indicate that the validation imagery is less than ideal,
318 especially for the lower CDOM values, because smoke effects may have been more widespread
319 than what was obvious for northern Minnesota. Nevertheless, the MAE values indicate
320 acceptable confidence in the resulting maps.

321

322 3.3 Geospatial analysis of statewide CDOM database

323 For geospatial analysis of CDOM at the ecoregion level, we calculated the mean CDOM
324 value for each waterbody (i.e. lakes, reservoirs and open-water wetlands) using the pixel-level
325 maps for 2015 and 2016 (Figures A1 and A2, respectively). These maps are also available in an
326 online LakeBrowser at <https://lakes.rs.umn.edu/>. Satellite-derived a_{440} values encompassed broad
327 ranges – from near undetectable (0.1 m^{-1}) to $\sim 25.5 \text{ m}^{-1}$ in both years. Standard deviations across
328 all waterbodies for both years were larger than the mean values, and median values were less
329 than the mean values (Table 3) indicating skewed distributions, with many more low-CDOM
330 waterbodies than high ones. Large differences in means, medians and statistical distributions
331 were found between the ecoregions, with high CDOM waters concentrated mainly in the NLF
332 and NMW. Nonetheless, a few waterbodies had high CDOM levels in all ecoregions in both
333 years. Standard deviations for a_{440} within all ecoregions were close to or larger than the mean
334 values, consistently indicating skewed distributions. Mean a_{440} and distributional statistics were
335 similar for the four southern and western ecoregions (NCHF, WCBP, NGP, LAP), and in all
336 cases 90% of their waterbodies had $a_{440} < \sim 6 \text{ m}^{-1}$.

337 Using the individual waterbody data for both years, we calculated the 2015-2016 mean
338 value for each waterbody and created a “lake-level” map (Figure 4). The associated statistical
339 distributions by ecoregion (Figure A3 and Table 4a) are similar to those described above for the
340 individual years. The mean a_{440} values for the two most northern ecoregions (NLF and NMW)
341 were higher than the means for the other four ecoregions in both years and for the average over
342 the time period, and the differences were even more pronounced for the 75% and 90% quantile
343 values. For example, 10% of the waterbodies in the NLF and NMW had average a_{440} values $>$

344 17.5 m⁻¹ in 2015-2016, but the 90% quantile values for the other four ecoregions were only 4.4-
345 5.4 m⁻¹ (Table 4a).

346 Waterbodies with high CDOM tend to have watersheds dominated by forests and
347 wetlands, but further inspection of high CDOM waterbodies in agricultural ecoregions (e.g.,
348 WCBP, NGP) indicated that they were mainly open-water wetlands with abundant aquatic
349 vegetation, where vegetation and bottom effects could affect R_{rs} and provide erroneous results
350 with satellite imagery methods. Ideally, pixels affected by aquatic vegetation or bottom sediment
351 would be masked because they are unsuitable for remotely sensed estimates of water quality.
352 Open-water wetlands were not well represented in the calibration dataset, however, because they
353 typically are ringed with emergent vegetation and are difficult to access. Because masking all
354 affected pixels is not always possible in large regional assessments, it is important to know the
355 limitations of the analysis and whether the satellite-based measurements are realistic for the
356 waterbodies that are being studied. Open-water wetlands tend to have high DOM concentrations,
357 which suggests that the satellite-based measurements are correct, but this issue needs further
358 investigation in future studies.

359 To minimize the effects of shallower open-water wetlands on CDOM statistical
360 distributions, we removed these waterbodies from the dataset and found distributions (Figure A4
361 and Table 4b) similar to those in Table 4a but with fewer high CDOM waters in the agricultural
362 ecoregions. Overall, mean a_{440} values and distributional statistics (except for maximum values)
363 were slightly lower in all ecoregions for the subset without open-water wetlands. For example,
364 for the four ecoregions with low average CDOM levels, the 90% quantile values were ~80% of
365 the corresponding values for the dataset that includes the shallow open-water wetlands (Table

366 4a), suggesting that on average, open-water wetlands tend to have slightly higher CDOM levels
367 than lakes and reservoirs.

368

369 *3.4 Potential sources of error*

370 Considering error levels indicated by MAE, atmospheric correction by MAIN resulted in
371 lower error than using OLI-SR (Table 2a, Figure 3), with overall MAE averages of 1.61 and 1.82
372 m^{-1} , respectively. MAE values for both correction methods increased across the three CDOM
373 ranges (low, medium, high) with MAIN and OLI-SR, and they represented ~25-30% of the
374 midpoint a_{440} values of each range. Although the model developed using L8/OLI imagery
375 worked reasonably well with our validation S2/MSI imagery, MAE values for the validation set
376 were consistently lower for L8/OLI than for S2/MSI. Further research with a larger dataset
377 would help to determine whether a separate S2/MSI model could improve the relationship with
378 measured data.

379 Although Brezonik et al. (2015) concluded that CDOM is generally stable on intra-
380 seasonal time scales, we found large fluctuations in CDOM in some highly colored lakes in
381 flowage systems (i.e., with large watersheds relative to lake areas) following large storm events
382 in summer of 2016. For this study, we used CDOM data within 30 days of image acquisition, but
383 because numerous storm events occurred in the state during summer of 2016, this could have
384 been too large a window for some highly colored flowage lakes and could account for some of
385 the overall error. The low R_{rs} signals from high-CDOM, low-suspended sediment water and
386 potential errors in atmospheric correction of such waters also could be contributing factors.

387 Differences between satellite and field measurements could originate from many sources
388 including (1) differences in spatial coverage (20-30 m pixels vs. a single grab sample), (2)

389 temporal variations in CDOM between the time of satellite overpass and sample collection, (3)
390 errors in collection and laboratory analyses, (4) differences that may arise in predicting measured
391 a_{440} from any retrieval model, and (5) satellite atmospheric correction errors. The latter
392 potentially may have been exacerbated by haze differences due to smoke in the validation vs. the
393 calibration dataset in this study. Given these issues and some uncertainties associated with the
394 representativeness of field data, it may be better simply to regard satellite-based methods as the
395 standard values for census-level CDOM data at regional scales. Ground-based measurements are
396 simply infeasible to gather at such spatial scales and short timescales. Of course, use of clear
397 imagery and appropriately calibrated models is essential for accurate results.

398

399 *3.5 Applications to research and management*

400 CDOM data for thousands of lakes measured at seasonal to annual time scales with the
401 satellite imagery methods described here are invaluable for lake management and research.
402 CDOM directly affects many important characteristics of lakes, such as temperature and light
403 regimes, primary production, and carbon cycling. It also affects many variables relevant to lake
404 management, including fisheries production and contaminant concentrations and reactivity.
405 Despite its important role, in situ data for CDOM are much more limited compared to other key
406 variables, such as chlorophyll and phosphorus (Stanley et al. 2019). Thus, frequent measurement
407 of CDOM at regional scales represents an important resource for research and management.

408 To illustrate the use of large-scale CDOM measurements, we examined the changes in
409 CDOM levels between two consecutive years with contrasting rainfall. Using the lake subset
410 (Table A3), we analyzed the change in a_{440} between 2015 and 2016. Comparison of precipitation
411 ranking maps for 2015 and 2016 shows major contrasts in hydrologic regimes between the years,

412 with 2015 fairly typical for most areas and 2016 unusually wet for most of the state, including
413 the NMW and NLF ecoregions (Figure A5). Comparing CDOM levels between years 2015 and
414 2016 (Table A4), we found that levels decreased by at least 3 m^{-1} in about 7% of the lakes in
415 agricultural ecoregions (LAP, NGP and WCBP), but levels increased in the ecoregions with
416 more forest and wetlands (Figure 5). Within the NMW and NLF ecoregions, 31% and 28% of the
417 lakes, respectively, had changes in $a_{440} \geq 3 \text{ m}^{-1}$, but only 5% of the lakes in the NCHF (a
418 transition ecoregion) changed more than 3 m^{-1} . It also is interesting to note that the mean and
419 median a_{440} values for the two high-CDOM ecoregions (NLF and NMW) increased substantially
420 from 2015 to 2016 (Table A3). In contrast, in almost all cases these statistics decreased in the
421 ecoregions with more agricultural and less forest/wetland land cover, apparently because of
422 dilution by increased precipitation. Although CDOM is generally stable at timescales of weeks to
423 months for many lakes, this analysis suggests that lakes in watersheds with large CDOM source
424 areas (i.e. forested wetlands) can exhibit substantial precipitation-driven variability. De Wit et al.
425 (2016) made similar conclusions based on analysis of long-term precipitation and CDOM
426 records in Scandinavia, and our calibration database also supports this conclusion. This example
427 provides an illustration of the utility of remote sensing methods to quantify CDOM changes in
428 response to environmental drivers such as precipitation, temperature and land cover changes.

429

430 **4. Conclusions**

431 This paper demonstrates that remote sensing using satellite-based sensors can play an
432 important role in providing census-level CDOM data over large areas at high temporal and
433 spatial resolution. The constellations of L8/OLI, upcoming Landsat 9/OLI and Sentinel 2/MSI

434 will greatly expand the capabilities to measure several optically-related water quality
435 characteristics, including CDOM.

436 Strong relationships for CDOM (a_{440}) were found using both MAIN and OLI-SR
437 atmospheric correction methods. Atmospheric correction using MAIN substantially improved
438 model performance, and has the advantage of being able to harmonize the R_{rs} values of L8/OLI
439 and S2/MSI, which will be important for automated image processing and near real-time
440 monitoring. The range of a_{440} values in our calibration dataset (0.2-32.5 m^{-1}) likely represents the
441 general distribution of CDOM throughout Minnesota.

442 Although further investigation of CDOM levels in shallow open-water wetlands of
443 agricultural areas should be undertaken, our results indicate that assessment of CDOM at
444 regional (statewide) scales is feasible using Landsat and Sentinel data. Such assessments can
445 provide the basis for numerous regional-scale analyses related to CDOM, such as (a) change
446 detection, as discussed above, (b) evaluating water clarity issues (e.g., Brezonik et al. 2019a), (c)
447 quantifying patterns of temperature structure, (d) estimating carbon storage and mercury levels in
448 lakes and wetlands, (e) predicting photochemical reaction rates in surface waters, and (f)
449 assessing water treatability metrics, such as chlorine demand and disinfection byproduct
450 formation (Chen et al. 2019). This approach could be extended to other regions, providing
451 similar results with appropriate model tuning and validation.

452

453 **Funding:** This work was supported in part by National Science Foundation grant (CBET
454 1510332), Minnesota Environmental and Natural Resources Trust fund, Minnesota Agricultural
455 Experiment Station, and University of Minnesota's U-Spatial Program, Sea Grant Program and
456 Office of the VP for Research and Retirees Association.

457

458 **Acknowledgments:** We thank the Minnesota Pollution Control Agency's lake water quality
459 assessment program and numerous collaborators, research staff, and students for assistance in
460 sample collection and analysis.

461

462 **Author Contributions:** Conceptualization of the study that led to this paper P.L.B., L.G.O., and
463 J.C.F., Conceptualization and methodology of remote sensing conducted by L.G.O., and B.P.P.
464 Formal statistical analysis done by L.G.O., and P.L.B. Field data planning analysis and collection
465 C.G.G., P.L.B., J.C.F., L.G.O., R.M.H. Writing and draft preparation done by L.G.O., P.L.B.,
466 J.C.F., B.P.P. Review and editing done by L.G.O., P.L.B., J.C.F., B.P.P., M.E.B., R.M.H. and
467 C.G.G. All authors contributed substantially to the produced work. All authors have read and
468 agreed to the published version of the manuscript.

469

470 **Conflicts of Interest:** The authors declare no conflict of interest.

471

472 **Supplemental Material:**

473

474 **References**

475 Ask, J., J. Karlsson, L. Persson, P. Ask, P. Byström, and M. Jansson. 2009. Terrestrial organic
476 matter and light penetration: Effects on bacterial and primary production in lakes. *Limnology*
477 and *Oceanography* **54**:2034-2040. <https://doi.org/10.4319/lo.2009.54.6.2034>.

478 Brezonik, P. L., R. W. Bouchard Jr., J. C. Finlay, C. G. Griffin, L. G. Olmanson, J. P. Anderson,
479 W. A. Arnold, and R. Hozalski. 2019a. Color, chlorophyll a, and suspended solids effects on

480 Secchi depth in lakes: implications for trophic state assessment. *Ecological Applications*
481 **29**:e01871. <https://doi.org/10.1002/eap.1871>.

482 Brezonik, P. L., J. C. Finlay, C. G. Griffin, W. A. Arnold, E. H. Boardman, N. Germolus, R. M.
483 Hozalski, and L. G. Olmanson. 2019b. Iron influence on dissolved color in lakes of the
484 Upper Great Lakes States. *PLoS ONE* 14(2): e0211979.
485 <https://doi.org/10.1371/journal.pone.0211979>.

486 Brezonik, P. L., K. Menken, and M. E. Bauer. 2005. Landsat-based remote sensing of lake water
487 quality characteristics, including chlorophyll and colored dissolved organic matter (CDOM).
488 *Lake Reserv. Manage.* 21(4): 373-382. <https://doi.org/10.1080/07438140509354442>.

489 Brezonik, P. L., L. G. Olmanson, J. C. Finlay, and M. E. Bauer. 2015. Factors affecting the
490 measurement of CDOM by remote sensing of optically complex inland waters. *Remote Sens.*
491 *Environ.* 157: 199-215. <http://dx.doi.org/10.1016/j.rse.2014.04.033>.

492 Chen, Y., W. A. Arnold, C. G. Griffin, L. G. Olmanson, P. L. Brezonik, and R. M. Hozalski.
493 2019. Assessment of the chlorine demand and disinfection byproduct formation potential
494 of surface waters via satellite remote sensing. *Water Research* 165: 115001.
495 <https://doi.org/10.1016/j.watres.2019.115001>.

496 Chen, J., W. Zhu, Y. Q. Tian, Q. Yu, Y. Zheng, and L. Huang. 2017. Remote estimation of
497 colored dissolved organic matter and chlorophyll-a in Lake Huron using Sentinel-2
498 measurements. *J. Appl. Remote Sens.* 11(3), 036007.
499 <https://doi.org/10.1117/1.JRS.11.036007>.

500 Corman, J. R., B. L. Bertolet, N. J. Casson, S. D. Sebestyen, R. K. Kolka, and E. H. Stanley.
501 2018. Nitrogen and Phosphorus Loads to Temperate Seepage Lakes Associated With

502 Allochthonous Dissolved Organic Carbon Loads. *Geophysical Research Letters* 45:5481-
503 5490. <https://doi.org/10.1029/2018GL077219>.

504 Creed, I. F., A.-K. Bergström, C. G. Trick, N. B. Grimm, D. O. Hessen, J. Karlsson, K. A. Kidd,
505 E. Kritzberg, D. M. McKnight, E. C. Freeman, O. E. Senar, A. Andersson, J. Ask, M.
506 Berggren, M. Cherif, R. Giesler, E. R. Hotchkiss, P. Kortelainen, M. M. Palta, T. Vrede, and
507 G. A. Weyhenmeyer. 2018. Global change-driven effects on dissolved organic matter
508 composition: Implications for food webs of northern lakes. *Global Change Biology* 24:3692-
509 3714. <http://dx.doi.org/10.1111/gcb.14129>.

510 de Wit, H. A., S. Valinia, G. A. Weyhenmeyer, M. N. Futter, P. Kortelainen, K. Austnes, D. O.
511 Hessen, A. Räike, H. Laudon, and J. Vuorenmaa. 2016. Current Browning of Surface Waters
512 Will Be Further Promoted by Wetter Climate. *Environ. Sci. Technol. Lett.* 2016, 3, 43.0-435.
513 <https://doi.org/10.1021/acs.estlett.6b00396>.

514 Finstad, A. G., T. Andersen, S. Larsen, K. Tominaga, S. Blumentrath, H. A. de Wit, H.
515 Tømmervik, and D. O. Hessen. 2016. From greening to browning: Catchment vegetation
516 development and reduced S-deposition promote organic carbon load on decadal time scales
517 in Nordic lakes. *Scientific Reports* 6:31944. <https://doi.org/10.1038/srep31944>.

518 Gordon, H.R. and M. Wang, 1994. Retrieval of water-leaving radiance and aerosol optical
519 thickness over the oceans with SeaWiFS: a preliminary algorithm. *Appl. Opt.* 33, 443-452.
520 <https://doi.org/10.1364/AO.33.000443>.

521 Gorelick, N., Hancher, M., Dixon, M., Ilyushchenko, S., Thau, D., Moore, R., 2017. Google
522 earth engine: planetary-scale geospatial analysis for everyone. *Remote Sens. Environ.* 202,
523 18–27. <https://doi.org/10.1016/j.rse.2017.06.031>.

524 Griffin, C. G., J. C. Finlay, P. L. Brezonik, L. G. Olmanson, and R. M. Hozalski. 2018.
525 Limitations on using CDOM as a proxy for DOC in temperate lakes. *Water Research* 144:
526 719–727. <https://doi.org/10.1016/j.watres.2018.08.007>.

527 Griffin, C. G., Frey, K. E., Rogan, J., and Holmes, R.M. 2011. Spatial and interannual variability
528 of dissolved organic matter in the Kolyma River, East Siberia, observed using satellite
529 imagery. *Journal of Geophysical Research – Biogeosciences*, 116(12), G03018.
530 <http://dx.doi.org/10.1029/2010JG001634>.

531 Houser, N. J. 2006. Water color affects the stratification, surface temperature, heat content, and
532 mean epilimnetic irradiance of small lakes. *Can. J. Fish. Aquat. Sci.* **63**:2447-2455.
533 <https://doi.org/10.1139/F06-131>.

534 Karlsson, J., P. Bystrom, J. Ask, P. Ask, L. Persson, and M. Jansson. 2009. Light limitation of
535 nutrient-poor lake ecosystems. *Nature* 460:506-508. <https://doi.org/10.1038/nature08179>.

536 Kirk, J. T. O. 2010. *Light and photosynthesis in aquatic ecosystems*, 3rd edition. Cambridge
537 University Press, Cambridge, UK. <https://doi.org/10.1017/CBO9781139168212>

538 Knoll, L. B., C. E. Williamson, R. M. Pilla, T. H. Leach, J. A. Brentrup, and T. J. Fisher. 2018.
539 Browning-related oxygen depletion in an oligotrophic lake. *Inland Waters* 8:255-263.
540 <https://doi.org/10.1080/20442041.2018.1452355>.

541 Kritzberg, E. S. 2017. Centennial-long trends of lake browning show major effect of
542 afforestation. *Limnology and Oceanography Letters* 2:105-112.
543 <https://doi.org/10.1002/lol2.10041>.

544 Kuhn, C., Valerio, A., Ward, N., Loken, L., Sawakuchi, H.O., Kampel, M., Richey, J., Stadler,
545 P., Crawford, J., Striegl, R., Vermote, E., Pahlevan, N., Butman, D., 2019. Performance of
546 Landsat-8 and Sentinel-2 surface reflectance products for river remote sensing retrievals of

547 chlorophyll-a and turbidity. *Remote Sens. of Environ.* 224, 104–118.
548 <https://doi.org/10.1016/j.rse.2019.01.023>

549 Kutser, T., D. C. Pierson, K. Y. Kallio, A. Reinart, and S. Sobek. 2005. Mapping lake CDOM by
550 satellite remote sensing. *Remote Sensing of Environment* 94:535-540.
551 <https://doi.org/10.1016/j.rse.2004.11.009>.

552 Kutser, T., L. Tranvik, and D. C. Pierson. 2009. Variations in colored dissolved organic matter
553 between boreal lakes studied by satellite remote sensing. *Journal of Applied Remote Sensing*
554 3(1):033538. <https://doi.org/10.1117/1.3184437>.

555 Menken, K., Brezonik, P. L., and Bauer, M. E. (2006). Influence of chlorophyll and humic color
556 on reflectance spectra of lakes: Implications for measurement of lake-water properties by
557 remote sensing. *Lake and Reservoir Management*, 22(3):179-190.
558 <https://doi.org/10.1080/07438140609353895>.

559 Olmanson, L. G., M. E. Bauer and P. L. Brezonik. 2008. Development and analysis of a 20-year
560 Landsat water clarity census of Minnesota's 10,000 lakes. *Remote Sens. Environ.* 112:4086-
561 97. <https://doi.org/10.1016/j.rse.2007.12.013>.

562 Olmanson, L.G., Bauer, M.E., and Brezonik, P.L. 2011. Evaluation of Medium to Low
563 Resolution Satellite Imagery for Regional Lake Water Quality Assessment. *Water Resources*
564 *Research*. 47:W09515. <http://dx.doi.org/10.1029/2011WR011005>.

565 Olmanson, L. G., P. L. Brezonik, J. C. Finlay, and M. E. Bauer. 2016a. Comparison of Landsat 8
566 and Landsat 7 for regional measurements of CDOM and water clarity in lakes. *Remote*
567 *Sensing of Environment* 185:119-128. <https://doi.org/10.1016/j.rse.2016.01.007>.

568 Olmanson, L. G., P. L. Brezonik, J. C. Finlay, and M. E. Bauer. 2016b. Regional-scale
569 measurement of colored dissolved organic matter in freshwater lakes by satellite imagery.

570 European Space Agency, Living Planet Symposium 2016, Prague, Czech Republic. May 9-
571 13, 2016.
572 http://lps16.esa.int/posterfiles/paper2319/Olmanson_CDOM_poster_ESA_LPS_final.pdf.
573 Accessed November 6, 2019.

574 Olmanson, L. G., P. L. Brezonik, and M. E. Bauer. 2014. Geospatial and temporal analysis of a
575 20-year record of Landsat-based water clarity in Minnesota's 10,000 lakes. *Journal of the*
576 *American Water Resources Association* 50(3): 748-761. <https://doi.org/10.1111/jawr.12138>.

577 Omernik, J. M. 1987. Ecoregions of the conterminous United States. *Annals of the Association*
578 *of American Geographers* 77(1):118–125. [https://doi.org/10.1111/j.1467-](https://doi.org/10.1111/j.1467-8306.1987.tb00149.x)
579 [8306.1987.tb00149.x](https://doi.org/10.1111/j.1467-8306.1987.tb00149.x).

580 Omernik, J. M. and G. E. Griffith. 2014. Ecoregions of the conterminous United States:
581 evolution of a hierarchical spatial framework. *Environmental Management* 54(6):1249–1266.
582 <https://doi.org/10.1007/s00267-014-0364-1>.

583 Page, B.P. Olmanson, L.G., and Mishra, D. R. 2019. A harmonized image processing workflow
584 using Landsat-8 and Sentinel-2 for mapping water clarity in optically complex lake systems.
585 *Remote Sens. Environ.* 231:111284. <https://doi.org/10.1016/j.rse.2019.111284>.

586 Pahlevan, N., Chittimalli, S., Balasubramanian, S., Vellucci, V., 2019. Sentinel-2/Landsat-8
587 product consistency and implications for monitoring aquatic systems. *Remote Sens. Environ.*
588 220:19-29. <https://doi.org/10.1016/j.rse.2018.10.027>.

589 Pahlevan, N., Schott, J., Franz, B.A., Zibordi, G., Markham, B., Bailey, S., Schaaf, C., Ondrusek,
590 M., Greb, S., and Strait, C., 2017a. Landsat 8 remote sensing reflectance (R_{rs}) products:
591 Evaluations, intercomparisons and enhancements. *Remote Sens. Environ.* 190, 1, 289-301.
592 <https://doi.org/10.1016/j.rse.2016.12.030>.

593 Pahlevan, N., Sarkar, S., Franz, B.A., Balasubramanian, S.V., and He, J., 2017b. Sentinel-2
594 MultiSpectral Instrument (MSI) data processing for aquatic science applications:
595 Demonstrations and validations. *Remote Sens. Environ.* 201, 47-56.
596 <https://doi.org/10.1016/j.rse.2017.08.033>.

597 Pilla, R. M., C. E. Williamson, J. Zhang, R. L. Smyth, J. D. Lenters, J. A. Brentrup, L. B. Knoll,
598 and T. J. Fisher. 2018. Browning-Related Decreases in Water Transparency Lead to Long-
599 Term Increases in Surface Water Temperature and Thermal Stratification in Two Small
600 Lakes. *Journal of Geophysical Research: Biogeosciences* 123(5):1651-1665.
601 <https://doi.org/10.1029/2017JG00432>.

602 Rampi, L.P., Knight, J. F., Bauer, M.E. (2016). Minnesota Land Cover Classification and
603 Impervious Surface Area by Landsat and Lidar: 2013 Update. Retrieved from the Data
604 Repository for the University of Minnesota, <http://doi.org/10.13020/D6JP4S>.

605 Ross, M. R. V., S. N. Topp, A. P. Appling, X. Yang, C. Kuhn, D. Butman, M. Simard, and T.
606 Pavelsy. 2019. AquaSat: a dataset to enable remote sensing of water quality for inland
607 waters. *Water Res. Research* **55**: 10012-10025. doi: 10.1029/2019WR024883

608 Snucins, E. and J. Gunn. 2000. Interannual variation in the thermal structure of clear and colored
609 lakes. *Limnology and Oceanography* 45:1639-1646.
610 <https://doi.org/10.4319/lo.2000.45.7.1639>.

611 Sobek, S., L. J. Tranvik, Y. T. Prairie, P. Kortelainen, and J. J. Cole. 2007. Patterns and
612 regulation of dissolved organic carbon: An analysis of 7,500 widely distributed lakes.
613 *Limnology and Oceanography* 52:1208-1219.

614 Solomon, C., S. Jones, B. Weidel, I. Buffam, M. Fork, J. Karlsson, S. Larsen, J. Lennon, J. Read,
615 S. Sadro, and J. Saros. 2015. Ecosystem Consequences of Changing Inputs of Terrestrial

616 Dissolved Organic Matter to Lakes: Current Knowledge and Future Challenges. *Ecosystems*
617 18:376-389. DOI: 10.1007/s10021-015-9848-y.

618 Stanley, E. H., S. M. Powers, N. R. Lottig, I. Buffam, and J. T. Crawford. 2012. Contemporary
619 changes in dissolved organic carbon (DOC) in human-dominated rivers: is there a role for
620 DOC management? *Freshwater Biology* 57:26-42. [https://doi.org/10.1111/j.1365-](https://doi.org/10.1111/j.1365-2427.2011.02613.x)
621 2427.2011.02613.x.

622 Stanley, E. H., S. M. Collins, N. R. Lottig, S. K. Oliver, K. E. Webster, K. S. Cheruvilil, and P.
623 A. Soranno. 2019. Biases in lake water quality sampling and implications for macroscale
624 research. *Limnology and Oceanography* 64(4):1572-1585. [https://doi.org/10.1002/lno.11136.](https://doi.org/10.1002/lno.11136)
625 [doi.org/10.1002/lno.11136.](https://doi.org/10.1002/lno.11136)

626 Thrane, J.-E., D. O. Hessen, and T. Andersen. 2014. The Absorption of Light in Lakes: Negative
627 Impact of Dissolved Organic Carbon on Primary Productivity. *Ecosystems* 17:1040-1052.
628 [https://doi.org/10.1007/s10021-014-9776-2.](https://doi.org/10.1007/s10021-014-9776-2)

629 Toming, K., T. Kutser, A. Laas, M. Sepp, B. Paavel, and T. Nõges. 2016. First Experiences in
630 Mapping Lake Water Quality Parameters with S2/MSI Imagery. *Remote Sensing* 8:640.
631 [https://doi.org/10.3390/rs8080640.](https://doi.org/10.3390/rs8080640)

632 Tsui, M. T. K., and J. C. Finlay. 2011. Influence of Dissolved Organic Carbon on
633 Methylmercury Bioavailability across Minnesota Stream Ecosystems. *Environmental Science*
634 & Technology 45:5981-5987. [https://doi.org/10.1021/es200332f.](https://doi.org/10.1021/es200332f)

635 Tyler, A., Hunter, P., Spyrakos, E., Groom, S., Maria Constantinescu, A., and Kitchen, J., 2016.
636 Developments in Earth observation for the assessment and monitoring of inland, transitional,
637 coastal and shelf-sea waters. *Sci. Total Environ.* 572, 1307–1321.
638 [https://doi.org/10.1016/j.scitotenv.2016.01.020.](https://doi.org/10.1016/j.scitotenv.2016.01.020)

639 Vanhellemont, Q., and Ruddick, K., 2015. Advantages of high quality SWIR bands for ocean
640 colour processing: Examples from Landsat-8. *Remote Sens. Environ.* 161:89-106.
641 <https://doi.org/10.1016/j.rse.2015.02.007>.

642 Vanhellemont, Q. and Ruddick, K., 2016. Acolite for Sentinel-2: Aquatic applications of MSI
643 imagery. *Proceedings of the 2016 ESA Living Planet Symposium, ESA Special Publication,*
644 *SP 740.*

645 Williamson, C. E., D. P. Morris, M. L. Pace, and A. G. Olson. 1999. Dissolved organic carbon
646 and nutrients as regulators of lake ecosystems: Resurrection of a more integrated paradigm.
647 *Limnology and Oceanography* 44:795-803.
648 https://doi.org/10.4319/lo.1999.44.3_part_2.0795.

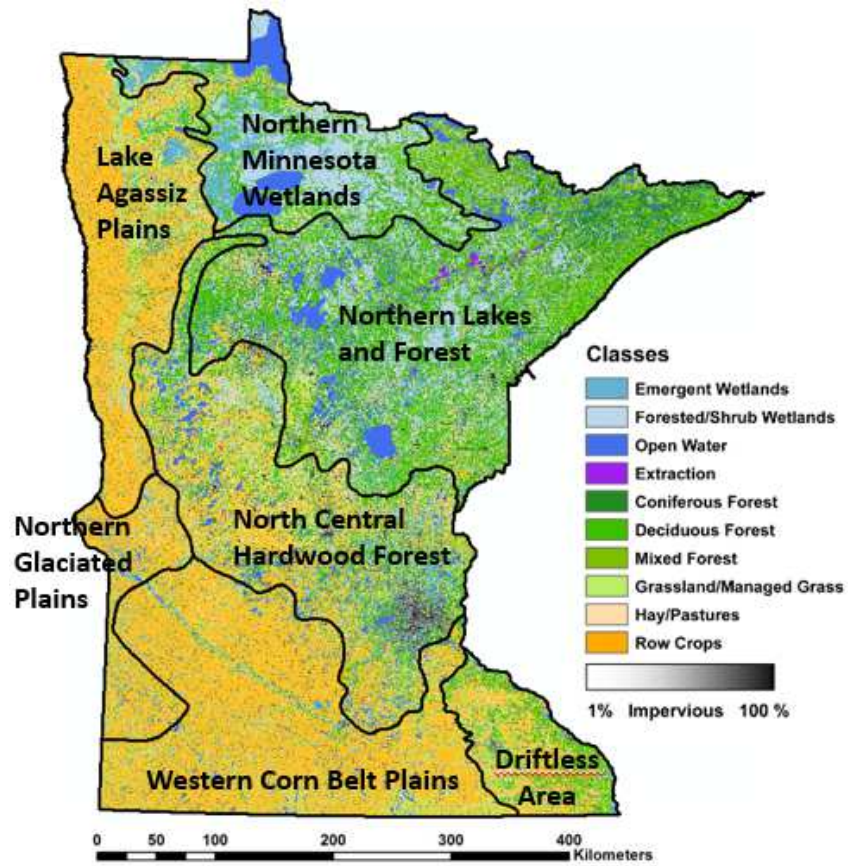


Figure 1. Minnesota 2013 land cover map (Rampi et al., 2016) with ecoregion boundaries (Omernik and Griffith, 2014).

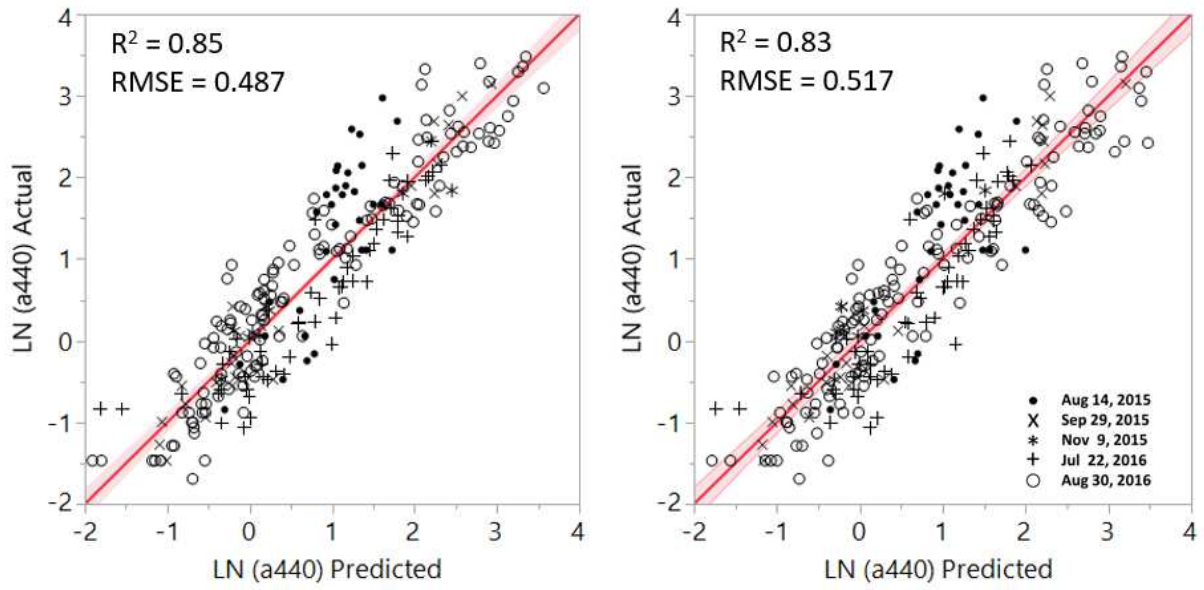


Figure 2. Landsat 8 CDOM models using MAIN (left) and SR (right) R_{rs} products.

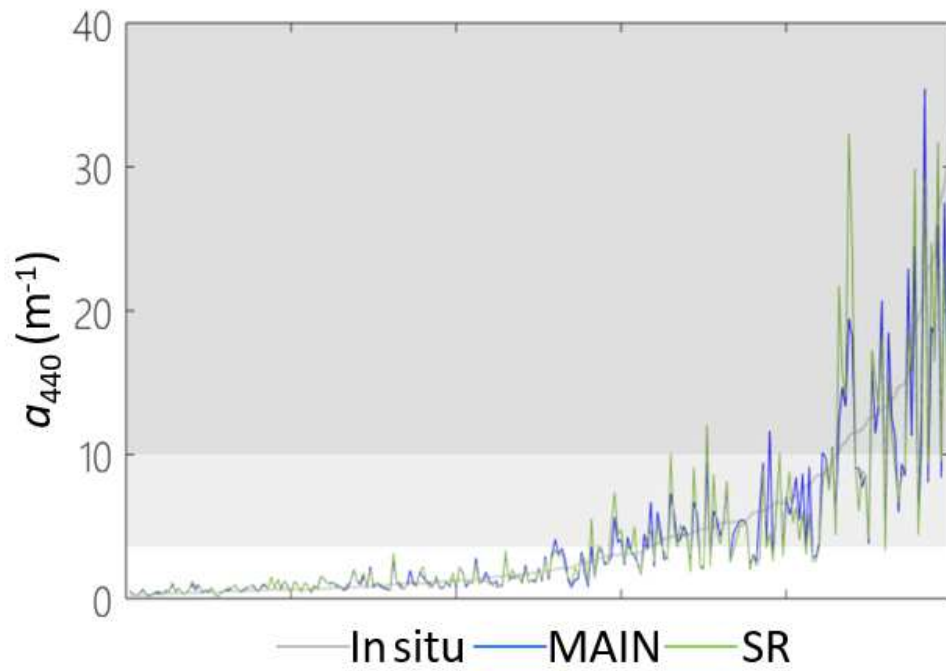


Figure 3. In situ a_{440} data sorted from low to high with resulting MAIN and SR model-derived a_{440} showing increasing divergence with increasing in situ a_{440} . The shading represents low, medium, and high CDOM levels.

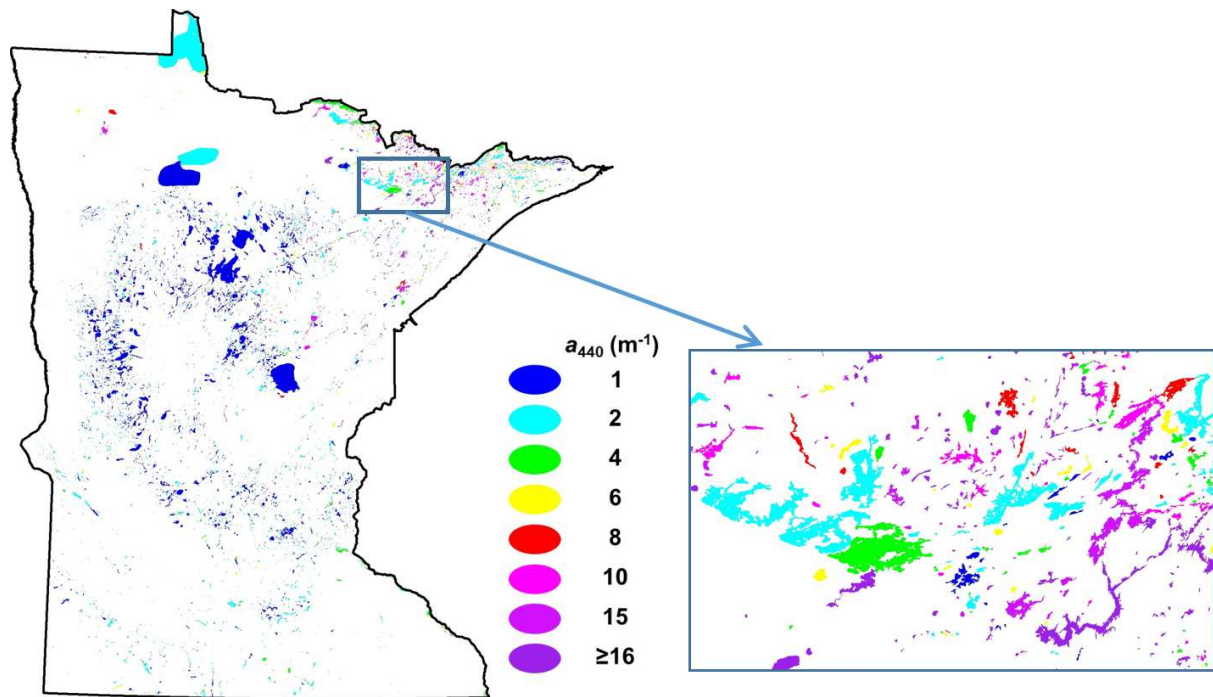


Figure 4. Mean 2015-2016 lake-level CDOM map with blowup of the Ely lakes area.

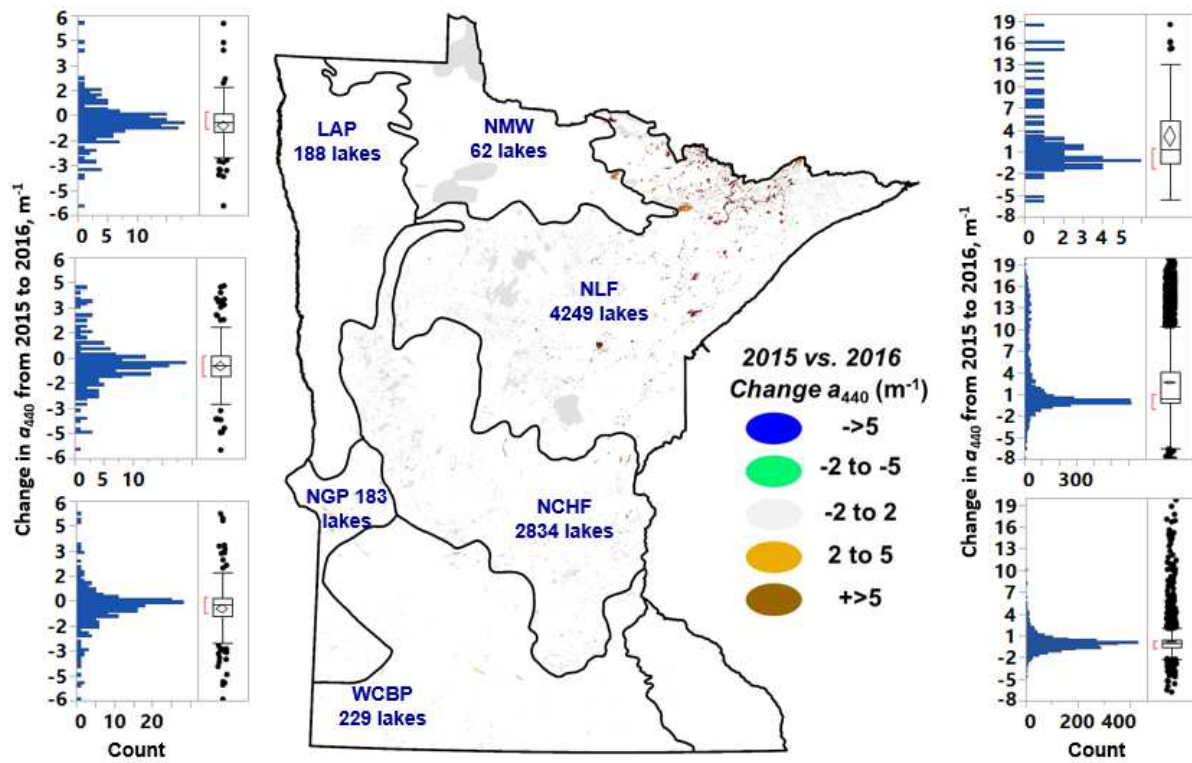


Figure 5. Percent change in a_{440} between 2015 compared to 2016 for each ecoregion. Increase of a_{440} between 2015 and 2016 due to increased precipitation in 2016 is focused in ecoregions with high coverage of forest and wetlands (NLF and NMW) while a_{440} decreases are in agricultural ecoregions (LAP, NGP and WCBP).

Table 1. Landsat 8 images used for calibration/validation and images used for 2015 and 2016-17 CDOM maps and associated number of ground-based (a_{440}) measurements.

Purpose	Sensor	Date	Path	Rows	N
calibration, 2015 map	L8/OLI	8/14/2015	26	27-28	33
2015 map	L8/OLI	9/20/2015	29	26-28	
calibration, 2015 map	L8/OLI	9/29/2015	28	26-30	24
2015 map	L8/OLI	11/7/2015	29	26-29	
calibration, 2015 map	L8/OLI	11/9/2015	27	26-30	9
calibration, 2016 map	L8/OLI	7/22/2016	27	26-29	53
calibration, 2016 map	L8/OLI	8/30/2016	28	26-28	131
2016 map	L8/OLI	11/4/2016	26	26-30	
2016 map	L8/OLI	11/9/2016	29	26-30	
2016 map	L8/OLI	11/11/2016	27	26-30	
2016 map	L8/OLI	5/13/2017	28	28-30	
2016 map	L8/OLI	9/9/2017	29	26-30	
Validation	S2/MSI	8/13/2018	MN_Middle	MN_N	95
Validation	L8/OLI	8/13/2018	27	28-30	62

Table 2. Error analysis for (a) L8 calibration dataset of MAIN and EROS SR CDOM models and (b) validation dataset for L8 and S2 models showing mean absolute error (MAE) in three ranges of a_{440} .

(a) Calibration data		CDOM range (a_{440}, m^{-1})		
Model	0-3	3-10	10-33	All
MAE (MAIN), m^{-1}	0.42	1.79	6.07	1.61
MAE (EROS SR), m^{-1}	0.43	2.05	7.10	1.82
N*	147	67	36	250

(b) Validation data				
L8-OLI MAE, m^{-1}; (N)	1.46 (49)	2.26 (12)	2.43 (1)	1.63 (62)
S2-MSI MAE, m^{-1}; (N)	1.58 (79)	2.90 (15)	2.93 (1)	1.80 (95)

* N is the number of data points in each range.

Table 3. Summary statistics and quantile information for 2015 and 2016 CDOM (a_{440} , m^{-1}) in waterbodies of Minnesota's six main ecoregions.

a). All measured waterbodies: 2015

Statistic	Ecoregion						
	All	NLF	NMW	NCHF	WCBP	NGP	LAP
Mean	3.54	4.83	6.45	2.05	3.25	2.99	2.89
Std dev	4.28	5.37	5.89	1.96	3.29	2.92	2.99
Std err mean	0.04	0.07	0.64	0.03	0.14	0.14	0.15
Minimum	0.16	0.16	0.71	0.20	0.25	0.55	0.30
Quantiles:							
10%	0.76	0.69	1.18	0.79	1.02	1.10	0.95
25%	1.15	1.17	2.22	1.07	1.55	1.52	1.30
Median (50%)	1.91	2.52	4.60	1.57	2.29	2.08	1.87
75%	3.82	6.69	7.96	2.32	3.57	3.30	3.19
90%	8.62	12.83	17.27	3.46	6.05	5.56	5.77
Maximum	25.50	25.50	25.50	25.50	25.50	25.50	23.60
N	10,782	5,081	83	4196	583	407	402

b) All measured waterbodies: 2016

Statistic	Ecoregion						
	All	NLF	NMW	NCHF	WCBP	NGP	LAP
Mean	4.90	7.53	9.70	2.58	2.50	2.49	2.13
Std dev	6.72	8.40	7.91	3.57	2.32	2.91	2.65
Std err mean	0.06	0.11	0.83	0.05	0.08	0.14	0.13
Minimum	0.10	0.20	0.51	0.21	0.32	0.10	0.20
Quantiles:							
10%	0.67	0.70	1.23	0.64	0.79	0.72	0.51
25%	1.03	1.22	2.93	0.92	1.18	1.00	0.81
Median (50%)	1.93	3.26	6.99	1.48	1.81	1.62	1.37
75%	4.81	11.89	16.69	2.59	2.85	2.87	2.29
90%	17.03	23.59	23.44	5.02	4.84	5.18	4.30
Maximum	25.50	25.50	25.50	25.50	19.44	25.50	23.70
N	11,565	5,337	91	4,451	748	411	406

Table 4. Summary statistics and quantile information for 2015-2016 average CDOM (a_{440} , m^{-1}) for all measured waterbodies and lakes and reservoirs (without open-water wetlands) only in Minnesota and its six main ecoregions.

a) All measured waterbodies

Statistic	Ecoregion						
	All	NLF	NMW	NCHF	WCBP	NGP	LAP
Mean	4.34	6.31	8.47	2.46	2.87	2.81	2.56
Std dev	5.34	6.63	6.70	2.94	2.36	2.69	2.64
Std err mean	0.05	0.09	0.70	0.04	0.09	0.13	0.13
Minimum	0.10	0.10	0.70	0.24	0.34	0.53	0.25
Quantiles:							
10%	0.80	0.74	1.54	0.80	1.00	1.02	0.79
25%	1.19	1.29	2.64	1.08	1.46	1.39	1.13
Median (50%)	2.03	3.20	6.11	1.60	2.21	1.91	1.72
75%	4.63	9.76	13.54	2.52	3.34	3.22	2.77
90%	12.79	17.54	17.62	4.40	5.38	5.37	5.16
Maximum	25.50	25.50	25.50	25.50	15.82	25.50	22.14
N	11,625	5,378	91	4,462	753	411	408

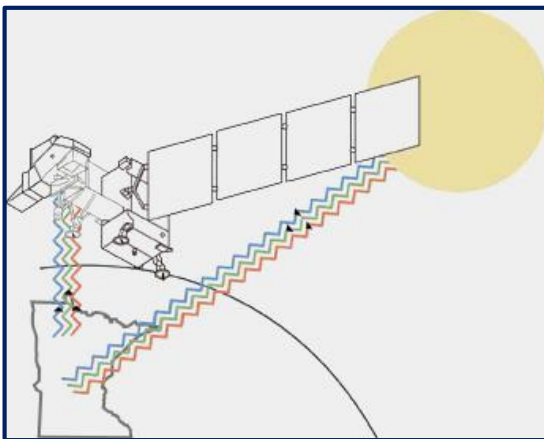
b) Lakes and reservoirs only

Statistic	Ecoregion						
	All	NLF	NMW	NCHF	WCBP	NGP	LAP
Mean	4.21	5.98	7.30	1.92	2.28	2.37	2.11
Std dev	5.34	6.43	6.56	1.98	1.67	1.66	2.17
Std err mean	0.06	0.10	0.81	0.04	0.10	0.12	0.16
Minimum	0.10	0.10	0.70	0.31	0.49	0.53	0.25
Quantiles:							
10%	0.75	0.71	1.29	0.76	0.91	0.88	0.71
25%	1.08	1.20	2.15	0.97	1.22	1.27	1.06
Median (50%)	1.84	2.92	5.38	1.40	1.78	1.87	1.44
75%	4.50	9.15	10.43	2.11	2.69	3.08	2.32
90%	12.97	16.89	17.40	3.35	4.28	4.55	4.07
Maximum	25.50	25.50	25.16	25.50	13.52	10.39	20.94
N	8,182	4,461	65	2,911	279	183	188

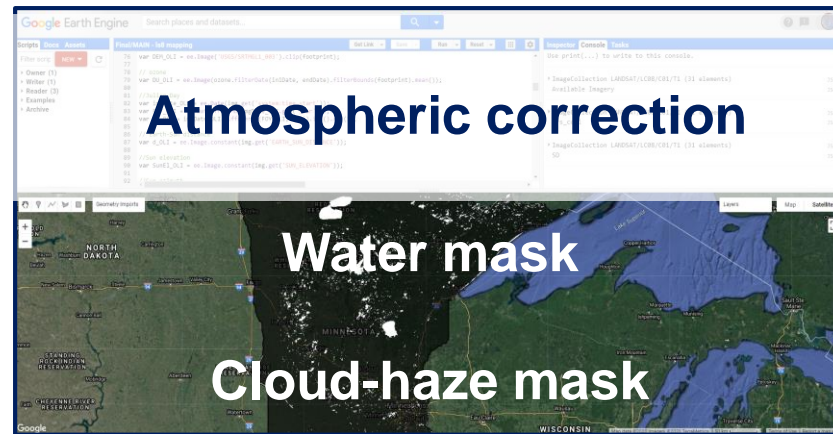
Collect samples to measure *in situ* CDOM



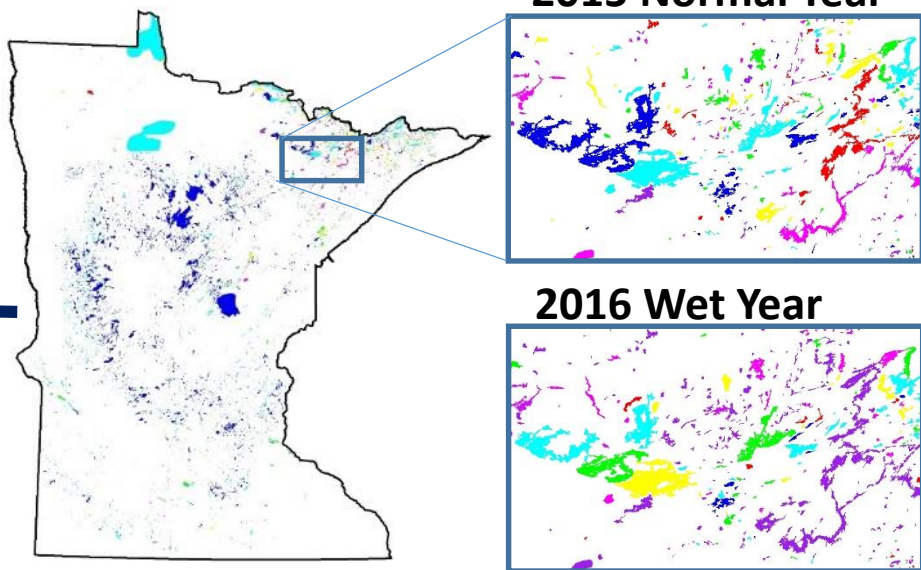
Landsat collects contemporaneous imagery



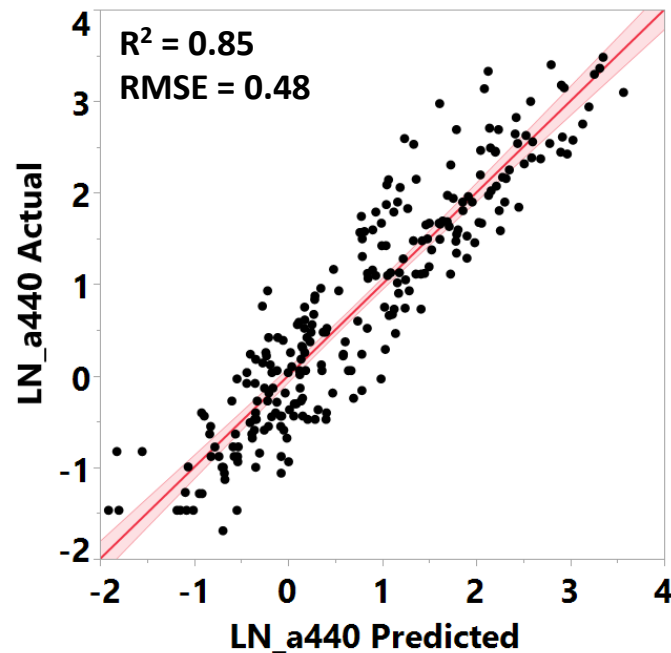
Preprocess images



Create CDOM maps



Build models



Spatial/temporal analysis

